Biophysical Chemistry 150 (2010) 54–63

Contents lists available at ScienceDirect

Biophysical Chemistry

journal homepage: http://www.elsevier.com/locate/biophyschem

Colloidal probe microscopy of membrane–membrane interactions: From ligand–receptor recognition to fusion events

Bärbel Lorenz [a], Rabea Keller [b], Eva Sunnick [a], Burkhard Geil [a], Andreas Janshoff [a,*]

[a] University of Goettingen, Institute of Physical Chemistry, Goettingen, Germany
[b] Max Planck Institute for Polymer Research, Mainz, Germany

ARTICLE INFO

Article history:
Received 15 December 2009
Received in revised form 5 February 2010
Accepted 7 February 2010
Available online 17 February 2010

Keywords:
Colloidal probe microscopy
Solid supported membranes
Hemifusion
Tether formation
Membrane–membrane interaction

ABSTRACT

A versatile model system to study membrane–membrane interactions in great detail is introduced. Based on colloidal probe microscopy with membrane covered spherical probes attached to tip-less cantilevers the interaction forces and adhesion energies are quantified down to single molecule resolution. Two opposing membranes equipped with ligands on one side and receptors on the other side were brought in contact at a defined load and pulled apart at constant velocity. Ni-NTA functionalized lipids served as receptors on the probe, while lipopeptides displaying short His-tags ($CGGH_6$ or $CGWH_6$) were incorporated in the planar supporting membrane on a silicon substrate. The rather intricate force distance curves were scrutinized in terms of breakthrough events upon contact of the probe with the surface, the overall work of adhesion, maximum adhesion force, as well as formation frequency, lifetime, and force of membrane tethers suggesting that hemifusion of the two opposing bilayers takes place.

1. Introduction

The mechanics and dynamics of plasma membranes play a crucial role in many cellular events such as adhesion, motility, membrane fusion, as well as exo- and endocytosis of mammalian cells. Particularly, membrane–membrane interactions display great versatility since molecular recognition, deformation, adhesion, pore formation, and fusion of lipid bilayers might occur depending on an intricate interplay between proteins, lipids, and forces. Among the considerable spectrum of processes involving membrane–membrane interactions, the understanding of cell–cell contacts [1], and membrane fusion is of particular interest. Membrane fusion occurs when two separate lipid membranes merge into a single continuous bilayer and plays a crucial role in embryogenesis, neurophysiology as well as viral infection [2–5]. Regardless of the process, the sequence of events, which is driven by subtle changes in free energy [3,4], requires almost without exception an initial specific recognition that triggers the subsequent dynamic response of the bilayer. This specific recognition between ligands on one membrane and the receptor displayed by the corresponding counterpart produces the initial molecular connection between two membranes, which eventually determines the fate of the membrane–membrane assembly, i.e. aggregation, hemifusion or full fusion [2–4].

Model systems of cellular membranes such as liposomes or supported membranes provide an excellent resource to investigate these processes in a quantitative manner under controlled conditions and defined composition. Investigation of membrane–membrane interactions in solution, however, bears the inevitable problem of aggregate formation due to cross-linked liposomes. As a consequence, precipitation and increased light scattering perturb or prevent a quantitative spectroscopic analysis.

Fusion is modulated by a number of external stimuli which control the crucial distance of the two membranes from each other and the hydration of the membranes such as force, calcium content, pH or other means that draw water from the contact zone such as polyethylene glycol [3,4]. When bilayers are separated below 1 nm, the energy of repulsion due to the pervasion of the hydration shell is assumed to drive fusion. It is widely accepted that formation of a fusion stalk and its expansion into a hemifusion diaphragm relaxes the hydration energy and hence provides the necessary driving force. Forces and, as a consequence, distances between two membranes can either be tuned by changing the interaction potential using charged lipids or varying the electrolyte or more directly using force probes such as optical/magnetic tweezers [6,7], the atomic force microscope [8] or the surface force apparatus (SFA) [9,10]. With properly functionalized probes, these methods allow to control composition of the two bilayers and the interaction force. While the SFA has been frequently used to identify and quantify van-der-Waals, electrostatic, repulsive hydration, and steric forces, it has in recent years also been applied to study more complex biological assemblies including membrane–membrane interactions [11,12]. Israelachvili and coworkers could assign hemifusion and full fusion events of two DMPC bilayers immobilized on PEI/mica to instabilities in force distances curves

* Corresponding author. Institut für Physikalische Chemie, Tammannstraße 6, D-37077 Göttingen, Germany. Tel.: +49 551 39 10633; fax: +49 551 39 14411.
E-mail address: ajansho@gwdg.de (A. Janshoff).

0301-4622/$ – see front matter © 2010 Elsevier B.V. All rights reserved.
doi:10.1016/j.bpc.2010.02.008

[13,14]. Full fusion was reported to occur only at very high joining pressure.

The cumbersome handling of the surface force apparatus and the lack of local information, however, prevented abundant dissemination to date. Atomic force microscopy, on the other hand, provides local information with a lateral resolution in the nanometer regime paired with an accessible force regime ranging from 10^{-11} to 10^{-6} N [8,15]. The drawback of conventional sharp tips for functionalization with lipid bilayers is their high curvature and therefore the difficulty to accomplish a successful functionalization. Particularly, the often undefined geometry of the tip renders conventional AFM cantilevers unsuitable to quantify membrane–membrane interactions.

Colloidal probe microscopy (CPM), a recent offspring of atomic force microscopy, combines the merits of a defined probe geometry and controllable surface functionalization with the potentiality to conduct site specific analysis of force distance curves [16,17]. In CPM a spherical particle is glued to a tip-less AFM cantilever essentially replacing the pyramidal tip with a spherical probe. The dimensions of the spherical (colloidal) particle are usually in between 1 and 20 μm in diameter. While CPM is frequently used for surface (friction) analysis under defined conditions, less applications are found in life sciences. Recently, Moy et al. investigated SNARE mediated fusion by membrane–protein functionalized surfaces and colloidal probes [18]. The authors interpret their results in terms of SNARE mediated full fusion of two opposing bilayers due to two consecutive instabilities observed in the approach curve. Previously, we established a setup that allows to determine the adhesion forces between the cytoskeleton and an ezrin covered membrane revealing a new route to ezrin activation via receptor binding [19].

Here, we report on a universal setup based on membrane covered silicon particles attached to tip-less cantilevers probing a solid supported membrane (SSM). The opposing membranes are either equipped with ligands or receptors allowing to study membrane–membrane interaction from the initial contact and formation of a non-covalent linkage to a possible (hemi)fusion and finally the dynamic action of the bilayers upon retraction creating membrane tethers that display the inherent mechanics of the two joint bilayers.

In our setup the colloidal probe with a diameter of 15 μm is coated with a phosphocholine membrane doped with phospholipids possessing a nitrilotriacetic acid headgroup (NTA) referred to as DXPC/Ni-NTA-DOGS capable of establishing strong non-covalent complexes with histidine oligomers in the presence of Ni^{2+}. Bilayers (DPPC/MCC-DPPE) deposited on flat silicon surfaces are functionalized with short His-tag moieties ($CGGH_6$ or $CGWH_6$) using recently introduced in situ coupling strategies [20–22]. By performing force–distance curves, which essentially brings the two bilayers in contact, we propose to induce hemifusion of the two membranes inferring from the occurrence of bilayer breakthrough events in the approach curve. After a short dwell time on the surface we move the cantilever backwards to separate the two membranes measuring the bonds that have been formed during the close proximity of the two membranes. Besides a typical adhesion force close to contact, we also observe formation of multiple tethers that exhibit lifetimes suggesting formation of lipid bridges.

2. Methods

Colloidal probe cantilevers were prepared by attaching a borosilicate glass microsphere ($Ø = (15 \pm 1)$ μm, Duke Scientific, Waltham, MA, USA) to an MLCT-C cantilever (Veeco, Santa Barbara, CA, USA) using epoxy resin (Epikote 1004, Shell, Hamburg, Germany). Attachment was monitored and carried out by using an upright light microscope with a 20× magnification lens equipped with a micromanipulator and a special device to attach the cantilever (MMO-203, Narishige, Tokyo, Japan). Prior to bilayer preparation on the colloidal probe, the cantilevers were cleaned in an argon plasma for 1 min.

Silicon wafers were cleaned by rinsing them with chloroform, isopropanol, and deionized water. Removal of native SiO_2 and controlled re-oxidation of the silicon wafer to an approximate oxide layer thickness of 3 nm was performed by using 1% hydrofluoric acid solution (15 min, room temperature (RT)), and an aqueous solution of ammonia and hydrogen peroxide (5:1:1; 15 min, 70 °C), respectively. For all measurements, unilamellar vesicles (SUVs) were prepared by extrusion using phosphate buffer (PB; Na_2HPO_4, 50 mM), pH 5.9 for lipid mixtures containing maleimide-functionalized vesicles, and pH 6.8 for Ni-NTA containing vesicles. SUVs were obtained by passing a suspension of multilamellar vesicles 31 times through a single polycarbonate membrane (pore diameter: 50 nm, Avestin, Mannheim, Germany). Lipid bilayers were prepared by incubating the SUV suspension on the substrates at RT followed by incubation above the corresponding main phase transition temperature (T_M) of the lipid, ($T_{M,DOPC} = -20$ °C, $T_{M,DPPC} = 41.5$ °C [23]; $c_{Lipid} = 0.1$ mg/ml of respective buffer, 30 min each step) and by thorough rinsing of the bilayer. For DOPC vesicles on the colloidal probe, incubation time was reduced to 15 min at RT. Planar bilayer formation and coverage of substrates was controlled by (confocal laser) fluorescence microscopy and atomic force microscopy imaging.

Lipid bilayers as spread on the colloidal probes were composed of 1,2-dioleoyl-*sn*-glycero-3-phosphocholine (DOPC), 1,2-dioleoyl-*sn*-glycero-3-[(N-(5-amino-1-carboxypentyl)iminodiacetic acid) succinyl] (nickel salt) (Ni-NTA-DOGS) and 2-(4.4-difluoro-5-methyl-4-bora-3a,4a-diaza-s-indacene-3-dodecanoyl)-1-hexadecanoyl-*sn*-glycero-3-phosphocholine (BODIPY C12-HPC, Invitrogen, Karlsruhe, Germany), in a molar ratio of 89:10:1. For functionalization of the flat silicon wafers, we used 1,2-dipalmitoyl-*sn*-glycero-3-phosphocholine (DPPC) as matrix lipid, and 1,2-dipalmitoyl-*sn*-glycero-3-phosphoethanolamine-N-[4-(p-maleimidomethyl)cyclohexane-carboxamide] (MCC-DPPE) in a concentration of 10 mol% as attachment site for the His-tag. In the case of DOPC as the matrix lipid MCC-DOPE (1,2-dioleoyl-*sn*-glycero-3-phosphoethanolamine-N-[4-(p-maleimidomethyl)cyclohexane-carboxamide) was used instead. Maleimide-functionalized DPPC bilayers were then incubated with acetylated $CGGH_6$ for 30 min at RT. $CGGH_6$-Ac ($M = 1100$ g/mol) was synthesized via Merryfield solid phase synthesis with Fmoc chemistry, purified via IEC and HPLC, and characterized by MALDI-ToF [22].

For force–distance measurements we used a commercial atomic force microscope (MFP3D, Asylum Research, Santa Barbara, CA, USA) and the above mentioned cantilevers with a nominal spring constant of 0.01 N/m. Spring constants were calibrated by using the thermal noise method and found to be approximately 0.03 N/m. Force–distance cycles were performed with a sample rate of 12.5 kHz, varying force load, dwell times, and pulling velocities. All measurements were performed in 50 mM phosphate buffer (pH = 6.8, RT) in a home-made measuring chamber. The integrity of lipid bilayers after force–distance measurements was controlled by fluorescence microscopy.

Liposome spreading and various subsequent binding events were also analyzed by extracting frequency and dissipation signals from quartz crystal microbalance measurements. We used a 5 MHz quartz with silicon dioxide coated electrodes (Qsense, Kista, Sweden). Prior to measurements, the quartz crystals were hydrophilized in oxygen plasma for 3 min. Measurements were performed in PB at 25 °C and vesicle concentrations of 0.1 mg/ml were applied. Vesicles consisting of DOPC with 10 mol% of MCC-DOPE and Ni-NTA-DOGS were spread on the resonators. Concentration of $CGWH_6$ for QCM-D measurements was 0.1 μmol/ml PB (pH = 6.8).

Texas Red-self-quenching experiments were carried out with DOPC vesicles (Ø = 50 nm) functionalized with 2 mol% MCC-DOPE, 10 mol% Texas Red DHPE (Sulforhodamine 101 DHPE, Sigma-Aldrich, Seelze, Germany) (population 1) or 2 mol% Ni-NTA-DOGS (population 2). Fluorescence spectroscopy with an excitation wavelength of

$\lambda_{exc} = 582$ nm was used to detect Texas Red DHPE dequenching at an emission wavelength of $\lambda_{em} = 605$ nm after addition of vesicle population 2 to population 1 (FP 6500, Jasco, Groß-Umstadt, Germany). Except for the lipid dyes, all lipids used were purchased from Avanti Polar Lipids, Alabaster, AL, USA.

3. Results and discussion

The interaction between membrane linked receptors and the corresponding membrane carrying ligands was probed with a setup schematically depicted in Fig. 1. A glassy sphere with a diameter of 15 µm attached to a tip-less cantilever is coated with a DOPC bilayer doped with 10 mol% of lipid molecules carrying Ni^{2+} nitrilotriacetic acid complexes (Ni-NTA) as head groups (DOPC/Ni-NTA-DOGS) [24]. Following a recently introduced protocol, short oligopeptides ($CGGH_6$) are coupled to maleimide-functionalized lipids embedded in the DPPC or DOPC matrix (DXPC) on the flat silicon wafer (DXPC/MCC-DXPE-$CGGH_6$) [22]. The two free binding sites of the hexagonally arranged nickel nitrilotriacetic acid (Ni-NTA) chelator serve as receptors for oligo-histidines displayed by the in situ coupled lipopeptides [25].

Fluid-phase DOPC bilayer were chosen for functionalization of the colloidal probe to ensure sufficient lateral mobility of the lipids and as a consequence to establish a satisfactory large number of recognition events during the membrane–membrane contact. Moreover, membranes in the fluid phase are more prone to fusion events due to substantially smaller bending moduli and area compressibilities. The spreading process on the glassy sphere and the integrity of the membranes were controlled by means of fluorescence microscopy. Fig. 2 shows a typical colloidal probe cantilever and the examination of its coverage with a fluorescently labeled DOPC bilayer (A and B) after addition of SUVs. Confocal laser scanning microscopy confirms a homogeneous coverage of the colloidal probe (inlay, Fig. 2B). Fluorescence recovery after photobleaching (FRAP) experiments carried out on the membrane covered spheres reveal that a continuous mobile bilayer could be deposited by means of vesicle spreading. Recovery of fluorescence in the bleached area was achieved after 100 s. The recovery was incomplete due to an exhausting membrane reservoir on the sphere. Diffusion coefficients were determined to be in the range of $(1.4 \pm 0.1)\,\mu m^2/s$ (Fig. 2C). We attribute the slightly smaller values compared to those found for fluid bilayers on planar substrates ($\sim 5\,\mu m^2/s$) [26,27] to the finite-sized spherical substrate imposing different boundary conditions. Force–distance curves with freshly prepared membrane probes taken on sufficiently hard surfaces show only single breakthrough events at

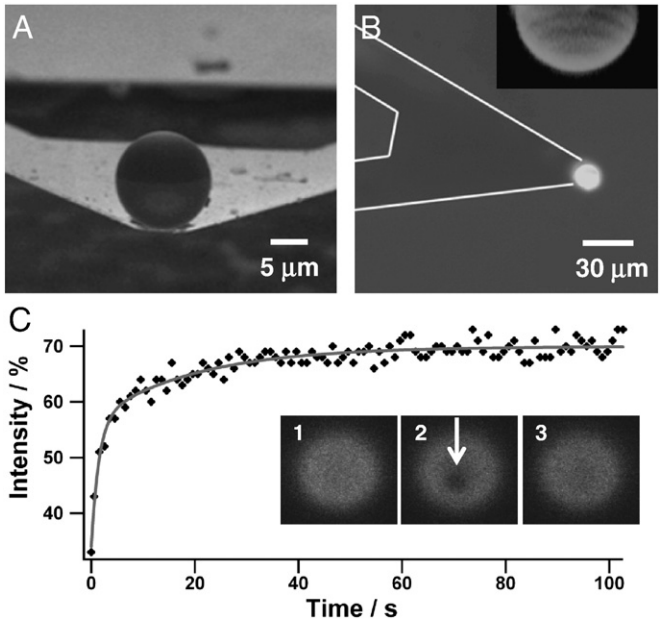

Fig. 2. A. SEM micrograph of a blank borosilicate microsphere attached to a triangular AFM cantilever. B. Epifluorescence image of the membrane coated colloidal probe cantilever (DOPC with BODIPY C12-HPC) and 3D reconstructed and deconvoluted confocal image of the colloidal probe (inset). C. Intensity profile of the fluorescence recovery after photobleaching reconstructed from the corresponding fluorescence images (1: before bleaching, 2: 800 ms, and 3: 40 s after bleaching). The mean diffusion coefficient determined from fitting of the intensity recovery as a function of time was $1.4 \pm 0.1\,\mu m^2/s$.

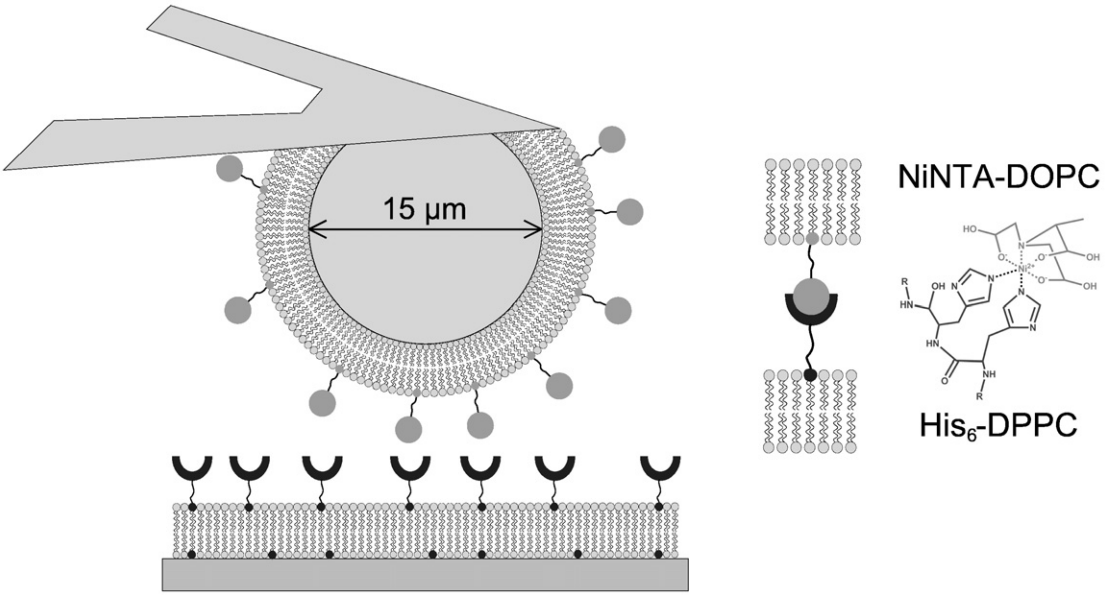

Fig. 1. Scheme of the experimental setup used in this study. A cantilever equipped with a colloidal probe is functionalized with a Ni^{2+}-nitrilotriacetate (Ni-NTA)-labeled DOPC bilayer (DOPC/Ni-NTA-DOGS, gray circles) by means of vesicle spreading. Force–distance curves are performed on a corresponding planar membrane spread on a flat silicon wafer and decorated with short His-tagged peptides (DXPC/MCC-DXPE-$CGGH_6$, dark gray crescent symbols).

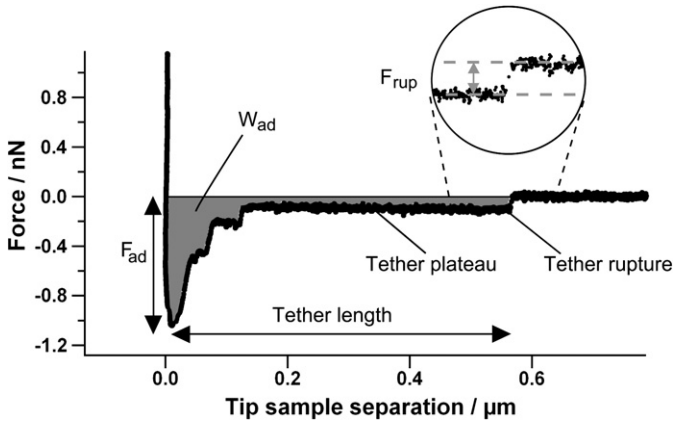

Fig. 3. Typical force retraction curve obtained after contacting a membrane (DOPC/Ni-NTA-DOGS, 90:10) covered colloidal probe with a planar bilayer equipped with His-tag peptides (DPPC/MCC-DPPE-$CGGH_6$, 90:10). Labels indicate the parameters that are generally obtained from the retraction curves. Work of adhesion (W_{ad}, gray area), maximum adhesion force (F_{ad}), number of tethers, tether length/lifetime and tether rupture forces F_{rup} are registered. The force curve has been recorded with a pulling speed of 2.5 µm/s and a dwell time on the surface of 1 s.

high force loads (8 nN force load; not shown) suggesting unilamellarity of the adsorbed bilayers on the spheres [28].

Force–distance cycles performed with the setup shown in Fig. 1 typically resulted in retraction curves of the colloidal probe from the surface as exemplarily depicted in Fig. 3. The retraction curve is characterized by a negative bending of the cantilever towards the surface as long as there are forces acting on the cantilever. While the breakage of initial interactions is characterized by a saw-tooth-like pattern, the extension of tethers far away from the surface is distinguished by force plateaus. These plateaus eventually disappear in a single relaxation step indicating tether rupture. The constant force observed in tether elongation is solely determined by intrinsic viscoelastic parameters associated with the bilayer and the retraction velocity [29,30]. In the case of multiple tether formation, the subsequent rupture of tethers produces a staircase-like retraction curve [31].

Information drawn from the force curves can be diverse. The approach curve contains information about possible breakthrough or membrane fusion events, while the retraction curves encompasses information about the overall work of adhesion, the maximum adhesion force, the lifetime of the tether, and the tether force. In the following section we will describe and discuss data analysis and consequences for possible scenarios of membrane–membrane interactions.

3.1. Adhesion force and work of adhesion

The most straightforward way to extract quantitative data from force retraction curves is to register the maximum adhesion force and the work of adhesion, which is essentially the integral as denoted in Fig. 3, and cast the individual values into a histogram. Appropriate control experiments were carried out to exclude that non-specific interactions interfere with the force response. Hence, we also monitored the maximum adhesion force F_{ad} and surface adhesion energy W_{ad} in the absence of the ligand $CGGH_6$ coupled to the planar membrane. We found a mean maximum adhesion force of (80 ± 190) pN for control experiments lacking the ligand $CGGH_6$ (Fig. 4A), while a more than 10 times higher adhesion force was found in presence of phospholipids displaying the ligand $CGGH_6$ ((880 ± 940) pN, Fig. 4B). The difference is even more pronounced for the adhesion energies, which is probably due to the augmented formation of membrane tethers once Ni-NTA bearing lipids form complexes with phospholipids displaying $CGGH_6$ tags. Notably, we use the term work of adhesion being distinct from the free energy of adhesion since the experiment is carried out under non-equilibrium conditions. Control experiments in the absence of $CGGH_6$ produce a work of adhesion of merely (2.7 ± 3.4) aJ in contrast to (97 ± 137) aJ for experiments

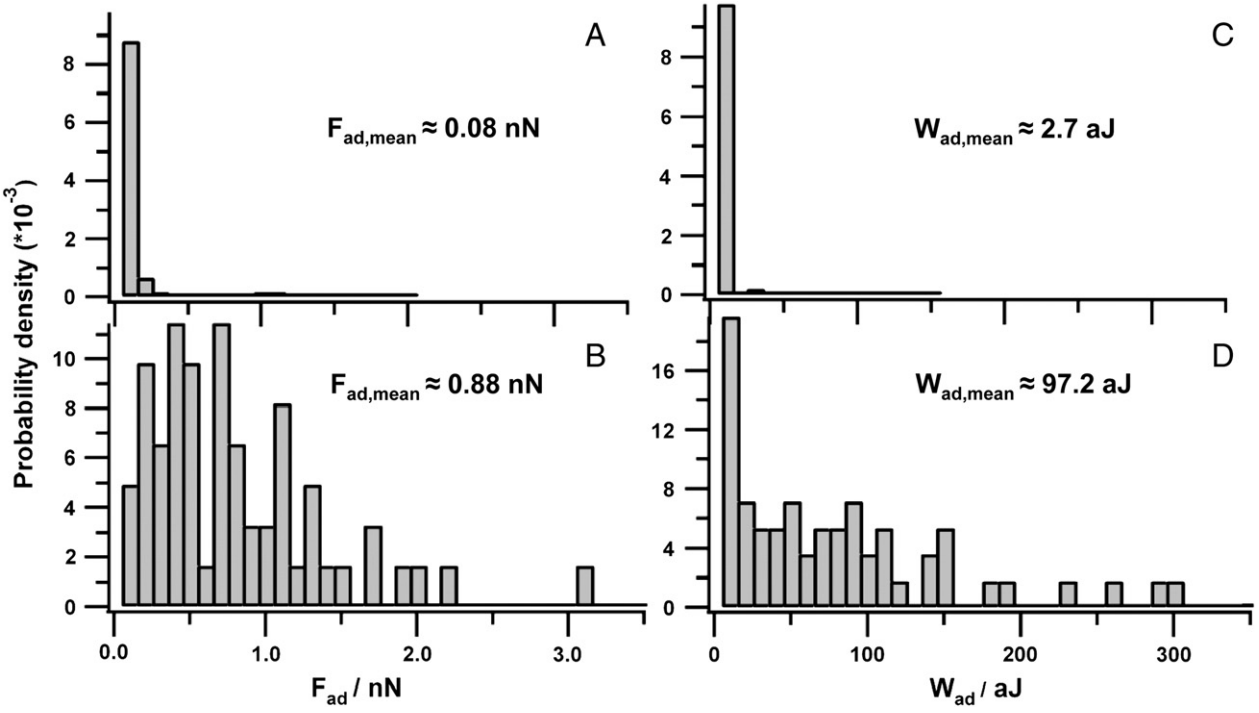

Fig. 4. Histograms of maximum adhesion forces F_{ad} (A, B) and work of adhesion W_{ad} (C, D) obtained from integration of the retraction force curve from the point of contact to the end of piezo travel as depicted in Fig. 3. Control experiments in the absence of $CGGH_6$ tags (A, C) show at least 10 times smaller values than CPM experiments allowing for the formation of ligand–receptor bonds between the two membranes (B, D). Force curves have been recorded with a pulling speed of 2.5 µm/s and a dwell time on the surface of 1 s. Data was pooled from 60 force curves with two different cantilevers for His-tag experiments and from 60 force curves with three different cantilevers for control experiments.

carried out in the presence of lipids functionalized with $CGGH_6$ (Fig. 4C,D).

The experiments clearly reveal that strong adhesion forces/energies result only if non-covalent linkages are allowed to form upon contact of the two membranes. It is, however, unclear whether unbinding of Ni-NTA–His-tag complexes is detected or membranes join at least partly thus forming a continuous leaflet which eventually ruptures upon extension.

3.2. Contact area and bilayer instabilities

It is instructive to first determine how many bonds may have been formed upon full contact of the two approaching membranes. The defined geometry of the colloidal probe permits a semi-quantitative analysis. After estimation of the approximate contact area between colloidal probe and the bilayer covered silicon wafer we will insert this information into a Monte Carlo simulation that eventually computes the number of possible contacts. For this purpose we assume that 10 mol% of the area is occupied by receptor molecules on the one membrane and the same percentage of ligands on the other side. Following the theory of Hertz, being the most vigorous simplification of all contact models and neglecting the impact of adhesive forces on the contact mechanics, the contact area depends on the external load force, the radius of the probe, and the Young's moduli E of the corresponding materials [32]. A further simplification arises by assuming that the indentation depth is below 10% of the bilayer thickness permitting us to consider the two membranes as semi-infinite bulk material with a Young's modulus of approximately 10 MPa (Poisson ratio: $\nu = 0.33$) [33]. The spheres used in our study have a radius of 7.5 μm and the load forces is at minimum 200 pN producing an overall indentation depth of 0.5 nm. We calculate a contact radius of $a = 60$ nm at a load force of 200 pN corresponding to a contact area of 21,900 nm^2. The number of lipid molecules within the contact are can be obtained from knowledge of the cross sectional area of a single lipid molecule ($A_{lipid} = 0.7\ nm^2$). Hence, a load force of merely 200 pN brings approximately 31,300 lipids in close contact. Since the membranes are doped with 10% of receptors or ligands, respectively, we can estimate that at most ~3000 molecular bonds can form allowing saturation of bonds. In order to obtain a more realistic number of ligand–receptor-linkages we performed a simple simulation based on two approaching surfaces with randomly placed ligands and receptors occupying an area of 10%. The number of irreversibly formed contacts is counted and lateral mobility is represented by a so-called affinity radius that increases with contact time according to the classical two-dimensional random walk of lipid molecules. Every pair at a distance smaller than the affinity radius is counted as a bond. Opening of bonds is not considered in order to simplify the procedure leading to the estimation of an upper limit of bonds. After 1 s dwell time of the colloidal probe in contact with the opposing membrane we can safely assume that indeed all possible bonds are formed at a load force of 200 pN (Fig. S1, supplementary materials).

CPM experiments with DOPC/Ni-NTA-DOGS (90:10) coated spheres approaching either planar DPPC (Fig. 5A) or DOPC (Fig. 5B) bilayers equipped with the corresponding ligand ($CGGH_6$) show similar trajectories on approach and retraction of the cantilever. In both cases bilayer instabilities are accompanied by formation of membrane tethers. The instabilities after contact are clearly visible and a sudden drop of the contact force occurs indicative of a mono- or bilayer breakthrough. DOPC membranes, however, are more prone to two subsequent breakthrough events (Fig. 5B) implying full fusion of the two DOPC bilayers, while DPPC bilayers are naturally more stable exhibiting single instabilities (Fig. 5A). We consider these observations, which correlate with the occurrence of tethers in the retraction curve, as a first indication that at least hemifusion events take place.

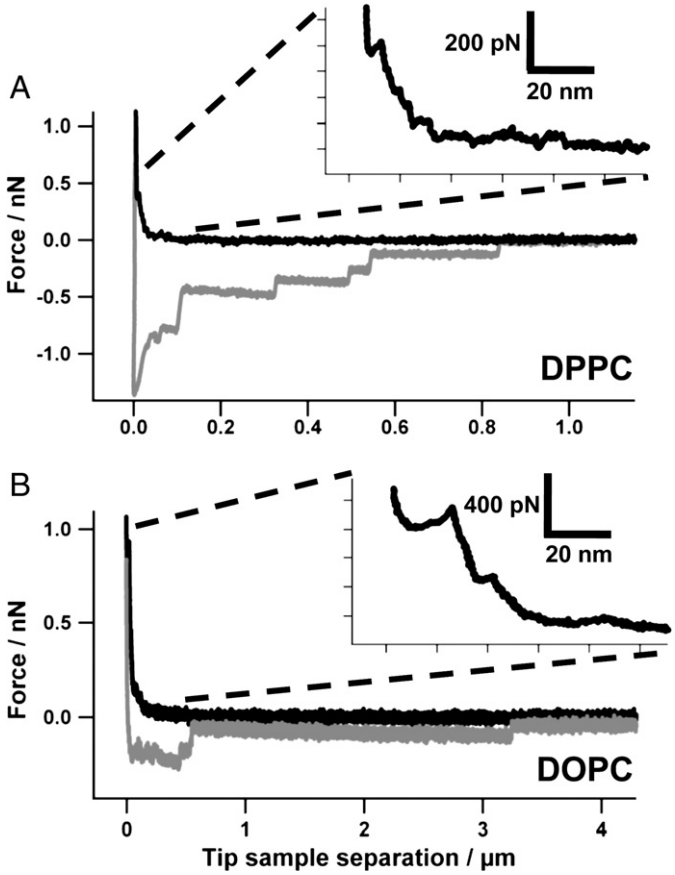

Fig. 5. Analysis of force–distance approach curves in the presence of $CGGH_6$ equipped lipids. While the colloidal probe approaches the surface, instabilities are detected within a distance of 20 nm to the surface. A. Approach and retraction curves of a colloidal probe covered with DOPC/Ni-NTA-DOGS (90:10) touching a DPPC/MCC-DPPE-$CGGH_6$ (90:10) bilayer on flat silicon. A single instability is found in the approach curve (inset) followed by multiple tethers upon retraction of the cantilever. B. Approach and retraction curves of a colloidal probe covered with DOPC/Ni-NTA-DOGS (90:10) touching a DOPC/MCC-DOPE-$CGGH_6$ (90:10) bilayer. Two instabilities are found in the approach curve (inset) followed by a single tether upon retraction of the cantilever.

3.3. Stochastic bond breakage or membrane fusion

Once the membranes have been brought into contact, two scenarios are conceivable upon retracting the colloidal probe from the substrate. The established bonds between the Ni-NTA lipids and the corresponding His-tag carrying lipids break as the force acting on them increases and the measured adhesion force reflects the stochastic nature of parallel bond breakage. Alternatively, membranes merge upon contact and the attractive forces are due to formation of continuous leaflets covering the colloidal probe and the silicon substrate. Fusion between the two membranes might be only partial and restricted to the outer leaflet, which is referred to as hemifusion. Full fusion requires both leaflets to join thus establishing a continuous bilayer.

The task is now to dissect the different scenarios by careful analysis of the force distance curves. One way would be to extrapolate the measured adhesion forces to the mean rupture force of a single bond and compare the results with the known potential of the Ni-NTA–His-tag complex from single molecule force experiments [34,35]. Previous studies on the stochastic bond breakage of Ni-NTA–His-tag bonds with an atomic force microscope provide us with the key parameters of the energy landscape simplified by a single prominent energy barrier, the off-rate k_{off} at zero force, the distance between the ground state and the activation barrier x_u, and the average bond strength at a particular

pulling speed. Following a protocol established by Beebe and coworkers should allow us to extrapolate our data (F_{ad}) to the failure of a single bond under external load assuming that the variance of adhesion forces obtained in the different experiments is only caused by a variation in the number of formed bonds [34]. Assuming further that the rupture events obey a Poisson distribution, one can plot the average force as a function of the variance and extract the dynamic bond strength of an individual bond from the slope. Trying this, we could not find the predicted linear relationship between the average force and its variance. As a consequence, the procedure of Beebe et al. is not purposeful in our case, either because the distribution of forces does not follow a Poisson distribution or because the governing connection between probe and sample is different from stochastic ligand–receptor bonds.

3.4. Tether formation

A second way to find out whether membranes have merged upon contact relies on registering of tether lifetimes. Tethers are lipid nanotubes with lipid bilayer walls and therefore possess an aqueous interior. They can be pulled out of membranes and rupture if the membrane reservoir that supplies the tether with lipid molecules is exhausted or the bond connecting the tether to the probe failures [36]. Once the tether is formed, its radius is constant and does only depend on the viscoelastic properties of the membrane [29,37]. Tethers are characterized by constant force upon extraction, which depends only on intrinsic mechanical parameters of the bilayer such as the bending modulus κ, the tension σ, and the shear viscosity η. Due to the viscous contribution the force depends also on the pulling speed v [30]:

$$F = 2\pi\sqrt{\kappa\sigma} - 2\pi\eta v \quad (1)$$

Eq. (1) can be used to extract intrinsic mechanical parameters from the tether pulling experiments. A plot of the tether force as a function of pulling velocity can be used to determine the apparent tension σ that also represents the adhesion of the bilayer to the colloidal sphere. We assume a bending modulus κ of 10^{-19} J corresponding to a fluid bilayer and thus find an apparent tension of 1.2 mN/m. The value corresponds well to recent findings from indentation of pore spanning bilayer and is attributed to large lateral tension due to strong adhesion to the surface [38]. The tether radius can readily been obtained from $r_{tether} = 2\pi\kappa / F_{tether}$ [39]. Assuming an equilibrium tether force F_{tether} of 80 pN, a tether radius of 6–10 nm is found.

The fact that tethers are formed upon pulling the probe away from the surface alone does not elucidate which bonds are strained and eventually failure. It just tells us that the membrane or at least one leaflet is lifted off from the support overcoming the adhesion force between the bilayer and the substrate. However, since the tether length is a measure of the bond's lifetime it can be used to estimate the off-rates at constant force $k_{off}(0)$ and compare the values to the known off-rates of the Ni-NTA–His tag bonds [35]. In many tether pulling experiments, it is assumed that the molecular bond attaching the probe or pulling device to the membrane remains intact. The lifetime of the bond is, however, a function of external force and the energy landscape, which is usually dominated by a single prominent energy barrier continuously lowered by the applied force ramp. Tethers can be used to create a constant force only depending on the mechanical properties of the membrane and the pulling velocity. Müller et al. introduced a method to measure the lifetime of single bonds at a defined constant force using membrane tethers pulled from cells at varying velocities [30]. We will adopt this procedure to judge whether stochastic bond rupture governs the process or hemifusion took place prior to retraction. In our CPM experiments usually multiple tethers were formed and a staircase force profile is observed (Fig. 3).

Analysis of the tether frequency (how many tethers are observed in a set of experiments) shows that in the control experiments (no $CGGH_6$) with a contact time of one second the maximum number of tethers in one retraction curve is only one (Fig. 6A). 85% of all the retraction curves showed no tether formation. In contrast, bilayers displaying $CGGH_6$ ligands showed a substantially higher tendency to form tethers. The highest number of tether plateaus observed in one retraction curve is eleven. There are also force curves observed in which no tethers are formed. This, however, correlates with a loss of membrane material from the probe due to successful tether formation prior to the actual pulling experiment (Figs. S2 and S3, supplementary material). This means that consecutive force curves are frequently devoid of tether events due to an exhausted membrane reservoir on the spheres. The mean number of tethers per retraction curve for control experiments is $n = 0.12$, whereas it is $n = 3.6$ for experiments with $CGGH_6$ ligands. The number of tethers increases with the dwell time of the probe in contact with the surface.

In the following, we describe a protocol developed by Müller and coworkers to obtain off rates from force clamp conditions (Eq. (1)). Hence, we monitored the lifetime of the tethers — as computed from the tether length by dividing by the pulling velocity — as a function of tether force. Fig. 7 shows the resulting histograms of tether lifetimes τ as a function of tether force adjusted by the pulling velocity. As expected, the lifetime increases with decreasing pulling speed. Assuming stochastic unbinding of a ligand–receptor pair, the unbinding probability $S(t)$ is described by a single exponential function:

$$S(t) = \exp\left(\frac{-t}{\tau}\right) \quad (2)$$

The corresponding probability density $W(t) = \frac{1}{\tau}\exp(\frac{t}{\tau})$ is fitted to the normalized histograms providing a mean lifetime of (1.27 ± 0.39) s for a pulling speed of 0.1 μm/s, (0.21 ± 0.02) s for 1 μm/s, and (0.11 ± 0.01) s for 2.5 μm/s. We also determined the lifetime of tethers at a particular force (last tethers) to determine $k_{off}(F) = \tau(F)^{-1}$. We arrived at (3.6 ± 0.4) s for a pulling speed of 0.1 μm/s, (0.32 ± 0.05) s for 1 μm/s, and (0.18 ± 0.02) s for 2.5 μm/s. Employing the Bell model that describes the obtained rates as a function of force allows us to determine both x_u, the potential width, and k_{off} at zero force ($k_{off}(0)$) [40]:

$$k_{off}(F) = k_{off}(0)\exp\left(\frac{x_u F}{k_b T}\right) \quad (3)$$

In the applied range of forces, a $k_{off}(0)$ was found to be $(0.63 \pm 0.44)\,s^{-1}$ and $x_u = (0.28 \pm 0.04)$ nm. Notably, we considered only the last and therefore single tethers in order to avoid undefined forces acting on each individual tether. Only the last tethers are subject to a defined force (plateau force). Although the lifetimes are thus slightly overestimated we can use them as an upper bound in the following argumentation. Comparing the off-rates at zero load force $k_{off}(0)$ and the distance from the ground state to the activation barrier x_u to available literature values ($k_{off}(0) = 0.07\,s^{-1}$, $x_u = 0.16$ nm) for the same ligand receptor couple it is evident that there is not even a remote resemblance between our data and literature values [35]. Particularly, the 10 times higher lifetime of Ni-NTA–His-tag bonds compared to our findings indicates that the anchorage of the tether is not established by one or more stochastic ligand–receptor bonds. In summary, we conclude that the linkage between the tether and the probe is most likely different from Ni-NTA chelating the corresponding His-tag ($CGGH_6$). We rather think that hemifusion took place due to the contact pressure exerted by the AFM facilitated by formation of strong ligand receptor bonds merging the membranes at least partly. This assumption is supported by the observation that tether

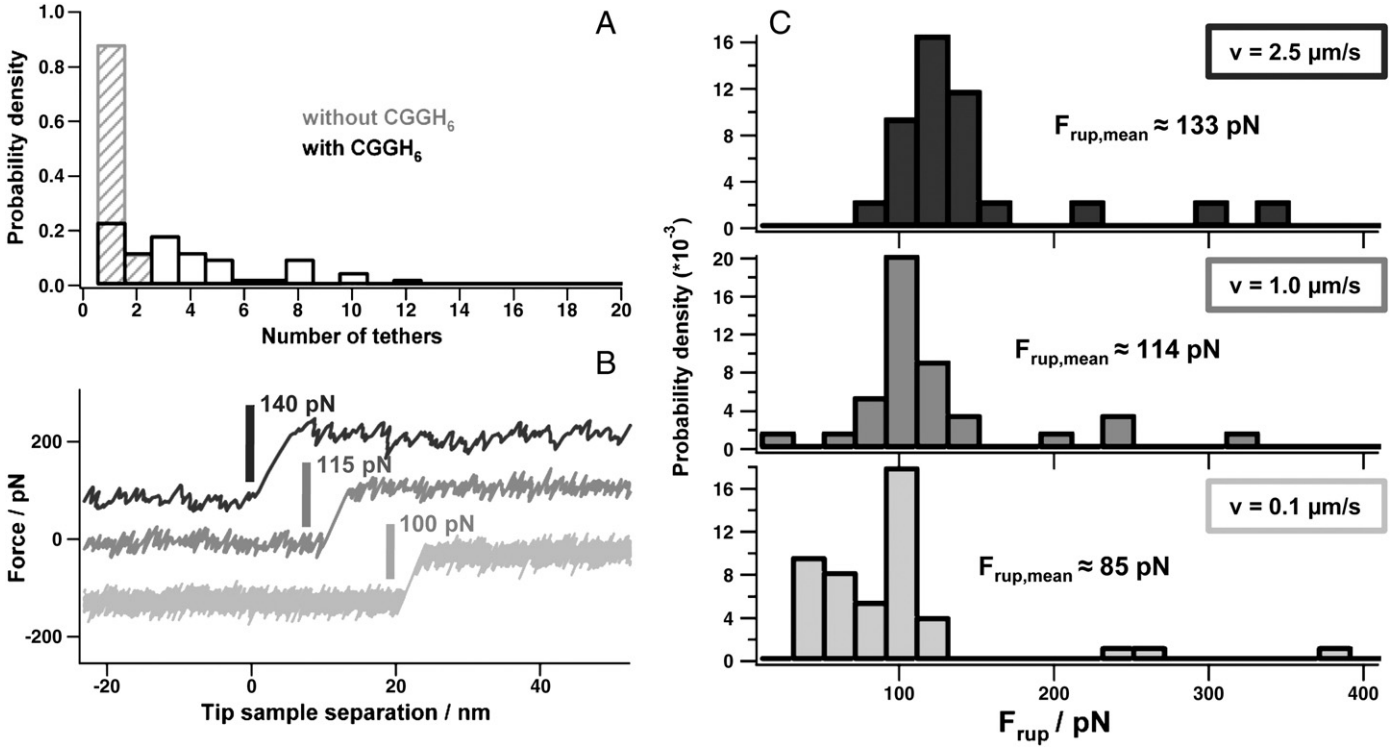

Fig. 6. A. Frequency of tether formation found in retraction curves with and without $CGGH_6$. The number of extracted nanotubes during one retraction process increases up to $n = 11$ upon addition of $CGGH_6$. B, C. Typical force retraction curves showing tethers with final rupture events at different pulling velocities and corresponding histograms of tether rupture forces at 2.5 µm/s (top), 1 µm/s (middle), and 0.1 µm/s (bottom). The distributions exhibit mean rupture forces of (133 ± 65) pN at 2.5 µm/s, (114 ± 59) pN at 1 µm/s, and (85 ± 68) pN at 0.1 µm/s. Increased pulling velocities lead to increased tether rupture forces as expected from Eq. (1). Histograms were calculated from measurements with two different cantilevers and 30 force curves for each velocity.

formation is related to single breakthrough events proceeding upon forced contact of the two membranes. As shown by Abdulreda et al. these small force jumps can be interpreted as hemifusion events [18].

According to analysis of approach curves hemifusion and fusion are abundantly observed for two DOPC covered surfaces in contact. Even in the absence of ligand receptor pairs the two membranes merge if contact is enforced by a joining pressure leading to the undercutting of a certain distance. In contrast, predominantly hemifusion is found for DOPC/DPPC systems but only if defined molecular bonds are formed upon approaching the colloidal sphere. Scrutiny of colloidal probes covered with functionalized DOPC bilayers after performing force experiments on corresponding DPPC membranes clearly shows missing patches of membrane on the colloidal probe (Fig. S3, supplementary materials). Fluorescence microscopy of DOPC/Ni-NTA-DOGS/Texas Red DHPE coated colloidal spheres after contact and tether formation with DPPC bilayers displaying $CGGH_6$ (DPPC/MCC-DPPE-$CGGH_6$) reveals that black, non-fluorescent areas are visible on the sphere implying that the DOPC bilayer has been irreversibly peeled off from the probe.

We conclude that rupture of tethers occurs due to stretching and failure of the DOPC bilayer while exhausting the reservoir on the silicon dioxide sphere. We assume that the DPPC bilayer on the flat silicon substrate remains largely unaffected upon retraction of the colloidal probe. Most likely, the fluid DOPC bilayer is peeled off the probe upon retraction forming a membrane tether, which is anchored in a hemifused fashion on the DPPC bilayer (see Figs. 10, S2, and S3). Obviously, the formation of ligand receptor bonds is necessary to overcome the barrier for hemifusion of DOPC with the gel-phase bilayer. Moreover, we found that roughly the same tether length was extracted regardless of the pulling velocity which we attribute to the finite lipid reservoir on the colloidal probe.

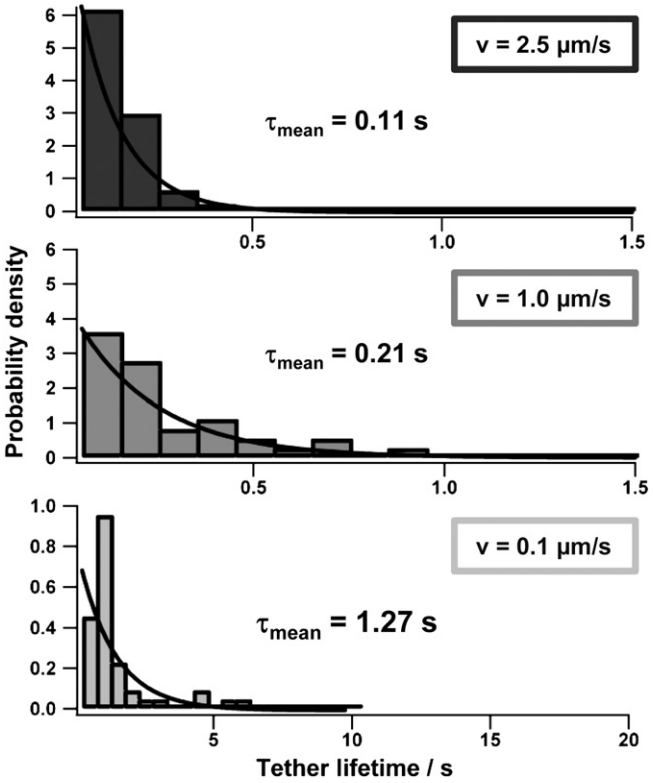

Fig. 7. Tether lifetimes τ at different pulling speeds. $\tau(F)$ increases with decreasing pulling speed (2.5 µm/s (top), 1 µm/s (middle), 0.1 µm/s (bottom)). Fitting of a monoexponential function results in mean lifetimes τ of (0.11 ± 0.01) s at 2.5 µm/s, (0.21 ± 0.02) s at 1 µm/s, and (1.27 ± 0.39) s at 0.1 µm/s pulling speed. Lifetimes are obtained from division of the tether length by the pulling velocity. Histograms were calculated from measurements with two different cantilevers and 40 force curves for each pulling velocity.

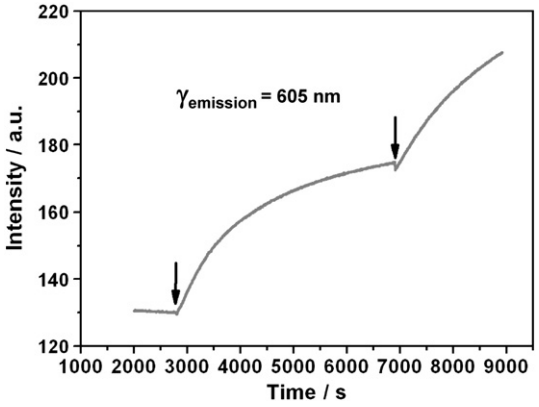

Fig. 8. Release of Texas Red DHPE self-quenching upon addition of Ni-NTA-functionalized vesicles (DOPC/Ni-NTA-DOGS (98:2); black arrows) to a population of $CGWH_6$-functionalized vesicles doped with Texas Red labeled lipids (DOPC/MCC-DOPE-$CGWH_6$/Texas Red DHPE, 88:2:10). While fluorescence intensity is constantly low at high fluorophor concentrations due to self-quenching, Texas Red emission increases upon addition of non-labeled vesicles functionalized with Ni-NTA due to lipid mixing.

3.5. Hemifusion of Ni-NTA-DOGS and MCC-DOPE-$CGGH_6$ functionalized liposomes in bulk experiments

In bulk experiments we found that two liposome populations consisting both of DOPC equipped with either Ni-NTA-DOGS or MCC-DOPE-$CGWH_6$ show hemifusion. Fig. 8 shows a Texas Red dequenching experiment, which is a popular assay to demonstrate fusion of vesicles [41]. More precisely, the experiments show that at least lipid mixing of the outer leaflets occurs upon contact of two liposomes. We found that Texas Red labeled lipids are self-quenched if fluorophor concentrations are higher than 4 mol% in a liposome. Hence, we doped one vesicle population with a very high fluorophor concentration of 10 mol% and functionalized these vesicles additionally with MCC-DOPE-$CGWH_6$ (10 mol%). Adding a second population of fluorophor-free vesicles functionalized with Ni-NTA lipids (Ni-NTA-DOGS, 10 mol%), a significant increase in fluorescence intensity was observed due to binding and subsequent fusion of the vesicles. The sudden increase in free area results in less self-quenching and hence the fluorescence intensity increases. Fluorescence microscopy measurements with the same kind of vesicle populations show an increase in vesicle size upon addition of Ni-NTA vesicles to $CGWH_6$-vesicles (data not shown). Importantly, typical content release assays such as the ANTS/DPX assay were unsuccessful excluding fully merged liposomes [42].

3.6. Docking of Ni-NTA-DOGS doped vesicles to MCC-DOPE-$CGWH_6$ containing SSMs

Irreversible binding of vesicles containing Ni-NTA-DOGS to a solid supported membrane equipped with MCC-DOPE-$CGWH_6$ ligands was found in a QCM-D experiment as detailed in Fig. 9. QCM-D measurements are ideally suited to detect the adsorption of viscoelastic bodies such as cells and liposomes and can be used to unequivocally detect bilayer formation due to rupture of vesicles on the surface [43–46]. Fig. 9 shows that short his-tagged peptides bind covalently to maleimide moieties of a spread DOPC/MCC-DOPE (90:10) bilayer as reported previously [22]. Addition of Ni-NTA-DOGS functionalized vesicles results in a large frequency drop associated with an increase in dissipation. These changes are due to an increase of viscoelastic mass on the oscillating quartz, which we assign to the binding of Ni-NTA-functionalized vesicles to $CGWH_6$ molecules on the membrane. A typical signature of bilayer spreading was not observed [43]. Adding of vesicles composed of DPPC rather than DOPC resulted in a significantly larger frequency shift (−155 Hz), which we attribute to the strong deformation experienced by the fluid DOPC liposomes resulting in smaller shifts of the acoustic load. Addition of EDTA to the bound DOPC/Ni-NTA-DOGS vesicles did not result in detachment of the liposomes due to complexation of Ni^{2+} as evident from an unchanged frequency response. We assign this finding to the hemifused state on the surface that renders the system insensible to removal of Ni^{2+}. Importantly, addition of EDTA to the adsorbed DPPC vesicles via the Ni-NTA–His tag bonding results in a small frequency increase (+36 Hz) due to desorption of vesicles. The better part of the attached vesicles, however, remains in contact.

3.7. Model perception

A number of different conceivable scenarios how (hemi)fusion takes place between the membrane coated colloidal probe and the planar solid supported membrane triggered by external force and formation of ligand receptor pairs exists. Fig. 10A–G shows a collection of schemes that illustrate possible structures of the formed tethers. Some of the scenarios can safely be excluded as deduced from the experimental evidence. The initial contact (A) leads to partial merging of the two bilayers (B) or to direct formation of a tether upon pulling (C). Retraction of the colloidal probe (C–G) might result in hemifusion of the outer leaflets of the two membranes (D, F, and G) or alternatively to full fusion (E). A subtlety occurs on the colloidal probe. The DOPC leaflet pointing to the sphere might detach (E and G) or remain in contact (D and F). Due to curvature penalty, structure (F) is not very likely to occur. The estimated tether radius of 6–10 nm favors structures C and G because less energy is paid for bending and hydrophobic chains are not exposed to the aqueous environment.

Since DPPC most likely does not participate in the tether formation at room temperature and hence does not act as a membrane reservoir upon pulling, we assume that the membrane reservoir consists exclusively of DOPC covering the colloidal sphere. This would also explain the relatively short tethers observed in the force retraction curves. We found considerably longer tethers when two DOPC membranes were brought into contact (Fig. 5). From the force distance curves alone we cannot exclude that multiple bonds between Ni-NTA lipids and the corresponding His-tag form and sustain the pulling force (Fig. 10C). The weakest link is the membrane tube itself. However, the additional bulk experiment (dequenching assay) and QCM-D experiments reveal that hemifusion (lipid mixing) has taken place. Taking all experimental evidence together, we can assume that Fig. 10G displays the most likely structure of the tether. In summary, we assume that the

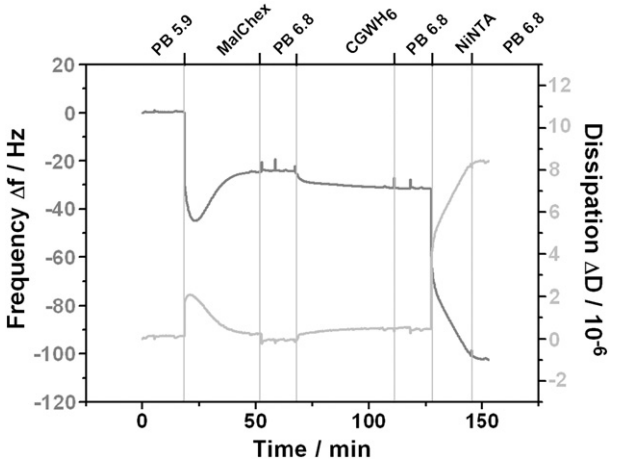

Fig. 9. Coupling of Ni-NTA-functionalized small unilamellar vesicles to a $CGWH_6$-functionalized bilayer investigated by QCM-D measurements. After spreading of a DOPC/MCC-DOPE (90:10) bilayer (initial drop of Δf) and the coupling of $CGWH_6$ (second frequency decrease), the frequency drops to −100 Hz upon the binding of Ni-NTA-functionalized DOPC (DOPC/Ni-NTA-DOGS, 90:10). The dissipation rises accordingly implying the attachment of a viscoelastic body.

Fig. 10. Schematic illustrations showing possible structures of the formed tethers upon retraction of the colloidal probe from the bilayer covered substrate. A. Initial contact resulting in partial fusion of the two bilayers (B). (C–G) Retraction of the colloidal probe results in tether formation. Note that hemifusion of the outer leaflets of the two membranes (D,F,G) or full fusion (E) are conceivable.

DOPC bilayer on the sphere feeds the tether, which is anchored in a hemifused manner onto the planar solid supported membrane.

Whether full fusion or merely hemifusion occurs depends also on the externally applied force and the fluidity of the bilayers. While coating both, the colloidal probe and the flat substrate with DOPC might favor full fusion, DPPC on either the colloidal probe or the flat substrate is likely to prevent the formation of fully merged membranes. Colloidal probe microscopy allows to widen the parameter space by allowing to control the force in a site specific fashion. While the approach curve provides a first cue whether fusion events took place just from the number of instabilities occurring upon forced contact, the retraction curve embodies even richer physics. Future experiments will include CPM measurements in conjunction with fluorescence microscopy such as total internal reflection fluorescence microscopy, which allows to monitor energy transfer of fluorophors while tethers are pulled from the contact regime.

4. Conclusions

Colloidal probe microscopy studies of membrane–membrane interactions are a versatile complement to traditional methods such as fusion assays based on liposomes and fluorescence techniques. It offers the unique possibility to investigate the forced contact between two bilayers, the involved instabilities upon merging, and the retraction process possibly characterized by stochastic unbinding events and the formation of membrane tethers. We have shown that even a simple system of ligand–receptor interactions bears rich physics and demands intricate models to explain the resulting new membrane structures. Depending on ligand receptor density, fluidity of the bilayer, and contact force various follow up reactions on the initial formation of non-covalent bonds are conceivable. We suspect that hemifusion of the outer leaflets is a highly probable pathway after contact of two membranes mediated by molecular recognition leading to membrane nanotubes.

Acknowledgements

B.L. gratefully acknowledges financial support from the state of Lower Saxony within the framework of the IMPRS of Physics of Biological and Complex Systems. We are also grateful for Gunnar Glasser's assistance in SEM imaging.

Appendix A. Supplementary data

Supplementary data associated with this article can be found, in the online version, at doi: 10.1016/j.bpc.2010.02.008.

References

[1] S.E. LaFlamme, A.P. Kowalczyk, Cell junctions: Adhesion, Development, and Disease, WILEY-VCH, 2008.
[2] R. Jahn, T.C. Sudhof, Membrane fusion and exocytosis, Annu. Rev. Biochem. 68 (1999) 863–911.
[3] L.V. Chernomordik, M.M. Kozlov, Mechanics of membrane fusion, Nat. Struct. Mol. Biol. 15 (2008) 675–683.
[4] L.V. Chernomordik, J. Zimmerberg, M.M. Kozlov, Membranes of the world unite! J. Cell Biol. 175 (2006) 201–207.
[5] S. Martens, H.T. McMahon, Mechanisms of membrane fusion: disparate players and common principles, Nat. Rev. Mol. Cell Biol. 9 (2008) 543–556.
[6] K.C. Neuman, S.M. Block, Optical trapping, Rev. Sci. Instrum. 75 (2004) 2787–2809.
[7] K.C. Neuman, A. Nagy, Single-molecule force spectroscopy: optical tweezers, magnetic tweezers and atomic force microscopy, Nat. Methods 5 (2008) 491–505.
[8] H.J. Butt, B. Cappella, M. Kappl, Force measurements with the atomic force microscope: technique, interpretation and applications, Surf. Sci. Rep. 59 (2005) 1–152.
[9] J.N. Israelachvili, Adhesion forces between surfaces in liquids and condensable vapors, Surf. Sci. Rep. 14 (1992) 109–159.
[10] D. Leckband, The surface force apparatus — a tool for probing molecular protein interactions, Nature 376 (1995) 617–618.
[11] M. Benz, T. Gutsmann, N.H. Chen, R. Tadmor, J. Israelachvili, Correlation of AFM and SFA measurements concerning the stability of supported lipid bilayers, Biophys. J. 86 (2004) 870–879.
[12] J.Y. Wong, C.K. Park, M. Seitz, J. Israelachvili, Polymer-cushioned bilayers. II. An investigation of interaction forces and fusion using the surface forces apparatus, Biophys. J. 77 (1999) 1458–1468.
[13] T.H. Anderson, Y.J. Min, K.L. Weirich, H.B. Zeng, D. Fygenson, J.N. Israelachvili, Formation of supported bilayers on silica substrates, Langmuir 25 (2009) 6997–7005.
[14] D.E. Leckband, C.A. Helm, J. Israelachvili, Role of calcium in the adhesion and fusion of bilayers, Biochemistry 32 (1993) 1127–1140.
[15] G. Binnig, C.F. Quate, C. Gerber, Atomic force microscope, Rev. Lett. 56 (1986) 930–933.
[16] I.L. Radtchenko, G. Papastavrou, M. Borkovec, Direct force measurements between cellulose surfaces and colloidal silica particles, Biomacromolecules 6 (2005) 3057–3066.
[17] C.E. McNamee, S. Armini, S. Yamamoto, K. Higashitani, Determination of the binding of non-cross-linked and cross-linked gels to living cells by atomic force microscopy, Langmuir 25 (2009) 6977–6984.
[18] M.H. Abdulreda, A. Bhalla, F. Rico, P.O. Berggren, E.R. Chapman, V.T. Moy, Pulling force generated by interacting SNAREs facilitates membrane hemifusion, Integr. Biol. 1 (2009) 301–310.
[19] M. Janke, A. Herrig, J. Austermann, V. Gerke, C. Steinem, A. Janshoff, Actin binding of ezrin is activated by specific recognition of PIP2-functionalized lipid bilayers, Biochemistry 47 (2008) 3762–3769.
[20] S. Schuy, E. Schafer, N.C. Yoder, S. Hobe, K. Kumar, R. Vogel, A. Janshoff, Coiled-coil lipopeptides mimicking the prehairpin intermediate of glycoprotein gp41, Angew. Chem., Int. Ed. 48 (2009) 751–754.
[21] S. Schuy, E. Schafer, N.C. Yoder, K. Kumar, R. Vogel, A. Janshoff, Lipopeptides derived from HIV and SIV mimicking the prehairpin intermediate of gp41 on solid supported lipid bilayers, J. Struct. Biol. 168 (2009) 125–136.
[22] S. Schuy, B. Treutlein, A. Pietuch, A. Janshoff, In situ synthesis of lipopeptides as versatile receptors for the specific binding of nanoparticles and liposomes to solid-supported membranes, Small 4 (2008) 970–981.
[23] http://www.lipidat.ul.ie/.
[24] L. Schmitt, C. Dietrich, R. Tampe, Synthesis and characterization of chelator-lipids for reversible immobilization of engineered proteins at self-assembled lipid interfaces, JACS 116 (1994) 8485–8491.
[25] E. Hochuli, H. Dobeli, A. Schacher, New metal chelate adsorbent selective for proteins and peptides containing neighboring histidine-residues, J. Chromatogr. 411 (1987) 177–184.
[26] L.K. Tamm, H.M. McConnell, Supported phospholipid-bilayers, Biophys. J. 47 (1985) 105–113.
[27] K.J. Seu, A.P. Pandey, F. Haque, E.A. Proctor, A.E. Ribbe, J.S. Hovis, Effect of surface treatment on diffusion and domain formation in supported lipid bilayers, Biophys. J. 92 (2007) 2445–2450.
[28] I. Pera, R. Stark, M. Kappl, H.J. Butt, F. Benfenati, Using the atomic force microscope to study the interaction between two solid supported lipid bilayers and the influence of synapsin I, Biophys. J. 87 (2004) 2446–2455.
[29] R.M. Hochmuth, J.Y. Shao, J.W. Dai, M.P. Sheetz, Deformation and flow of membrane into tethers extracted from neuronal growth cones, Biophys. J. 70 (1996) 358–369.
[30] M. Krieg, J. Helenius, C.P. Heisenberg, D.J. Muller, A bond for a lifetime: employing membrane nanotubes from living cells to determine receptor–ligand kinetics, Angew. Chem., Int. Ed. 47 (2008) 9775–9777.
[31] M.Z. Sun, J.S. Graham, B. Hegedus, F. Marga, Y. Zhang, G. Forgacs, M. Grandbois, Multiple membrane tethers probed by atomic force microscopy, Biophys. J. 89 (2005) 4320–4329.
[32] H. Hertz, Über die Berührung fester elastischer Körper, J. Reine Angew. Math. 92 (1882) 156.
[33] S. Kunneke, D. Kruger, A. Janshoff, Scrutiny of the failure of lipid membranes as a function of headgroups, chain length, and lamellarity measured by scanning force microscopy, Biophys. J. 86 (2004) 1545–1553.
[34] J.M. Williams, T.J. Han, T.P. Beebe, Determination of single-bond forces from contact force variances in atomic force microscopy, Langmuir 12 (1996) 1291–1295.
[35] C. Verbelen, H.J. Gruber, Y.F. Dufrene, The NTA-HiS(6) bond is strong enough for AFM single-molecular recognition studies, J. Mol. Recognit. 20 (2007) 490–494.
[36] D. Raucher, M.P. Sheetz, Characteristics of a membrane reservoir buffering membrane tension, Biophys. J. 77 (1999) 1992–2002.
[37] R.E. Waugh, J. Song, S. Svetina, B. Zeks, Local and nonlocal curvature elasticity in bilayer membranes by tether formation from lecithin vesicles, Biophys. J. 61 (1992) 974–982.
[38] I. Mey, M. Stephan, E.K. Schmitt, M.M. Muller, M. Ben Amar, C. Steinem, A. Janshoff, Local membrane mechanics of pore-spanning bilayers, JACS 131 (2009) 7031–7039.
[39] P. Nassoy, D. Cuvelier, R. Bruinsma, F. Brochard-Wyart, Nanofluidics in cellular tubes under oscillatory extension, Epl 84 (2008).
[40] G.I. Bell, Models for specific adhesion of cells to cells, Science 200 (1978) 618–627.
[41] J.M. Johnson, T. Ha, S. Chu, S.G. Boxer, Early steps of supported bilayer formation probed by single vesicle fluorescence assays, Biophys. J. 83 (2002) 3371–3379.
[42] H. Ellens, J. Bentz, F.C. Szoka, H^+-induced and Ca^{2+}-induced fusion and destabilization of liposomes, Biochemistry 24 (1985) 3099–3106.
[43] R.P. Richter, R. Berat, A.R. Brisson, Formation of solid-supported lipid bilayers: an integrated view, Langmuir 22 (2006) 3497–3505.
[44] S. Faiss, E. Luthgens, A. Janshoff, Adhesion and rupture of liposomes mediated by electrostatic interaction monitored by thickness shear mode resonators, Eur. Biophys. J. Biophys. 33 (2004) 555–561.
[45] E. Luthgens, A. Herrig, K. Kastl, C. Steinem, B. Reiss, J. Wegener, B. Pignataro, A. Janshoff, Adhesion of liposomes: a quartz crystal microbalance study, Meas. Sci. Technol. 14 (2003) 1865–1875.
[46] B. Pignataro, C. Steinem, H.J. Galla, H. Fuchs, A. Janshoff, Specific adhesion of vesicles monitored by scanning force microscopy and quartz crystal microbalance, Biophys. J. 78 (2000) 487–498.